Available online at www.sciencedirect.com
ScienceDirect
Spectrochimica Acta Part A 67 (2007) 916–929
SPECTROCHIMICA ACTA PART A
www.elsevier.com/locate/saa

Synthesis, characterization and properties of some divalent metal(II) complexes: Their electrochemical, catalytic, thermal and antimicrobial activity studies

Mehmet Tümer [a,*], Duygu Ekinci [b], Ferhan Tümer [b], Akif Bulut [a]

[a] *University of Kahramanmaraş Sütçü Imam, Faculty of Science and Arts, Department of Chemistry, 46100 Kahramanmaraş, Turkey*
[b] *Atatürk University, Faculty of Science and Arts, Department of Chemistry, Erzurum, Turkey*

Received 5 January 2006; received in revised form 31 August 2006; accepted 11 September 2006

Abstract

In this study, we synthesized the amine compound 2-(2-aminoethyliminomethyl)phenol (H_3A) as the starting material, and then we prepared the polydentate Schiff base ligands from the reactions of the amine compound (H_3A) with phtaldialdehyde (H_2L), 4-methyl-2,6-di-formlyphenol (H_3L^1) and 4-*t*-butyl-2,6-di-formylphenol (H_3L^2) in the ethanol solution. Moreover, the complexes Cd(II), Cu(II), Co(II), Ni(II), Zn(II) and Sn(II) of the ligands H_2L, H_3L^1 and H_3L^2 have been prepared. All compounds have been characterized by the analytical and spectroscopic methods. In addition, the magnetic susceptibility and molar conductance measurements have been made. The catalytic properties of the mono- and binuclear Co(II) and Cu(II) complexes have been studied on the 3,5-di-*tert*-butylcatechol (3,5-DTBC) and ascorbic acid (aa) as a substrate. The oxidative C–C coupling properties of the Co(II) and Cu(II) complexes have been investigated on the sterically hindered 2,6-di-*tert*-butylphenol (dtbp). The antimicrobial activity properties of the ligands and their mono- and binuclear complexes have been studied against the bacteria and fungi. The results have been compared to the antibacterial and fungi drugs. The TGA curves show that the decomposition takes place in three steps for all complexes. Electrochemical properties of the complexes Cu(II) and Ni(II) have been investigated for the first time in acetonitrile by cyclic voltammetry.

Keywords: Schiff base; Electrochemical; Catalytic; Thermal and antimicrobial activity

1. Introduction

The metal complexes with Schiff bases as ligands have been playing an important role in the development of coordination chemistry as a whole. However, it was not until the 1950s that concrete and rapid advances in this field became evident. In the early days, the main efforts were directed toward synthesis and characterization of rather fundamental complexes, which do not look striking nowadays but were strongly needed in those days. Some of typical examples included metal complexes of the following types: M(II)(X–Sal–NR)$_2$, M(III)(X–Sal–NR)$_3$, and so on, where X–Sal–NR denotes bidentate Schiff bases [1]. To cite another example, it was regarded as significant to synthesize complexes of the formula Co(X–Sal–NR)$_3$, R: *i*-Pr, where X: 5-Br and 5-NO$_2$ [2]; it had been believed that the formation of these complexes would be obstructed by the steric constraint due to the bulky *i*-Pr group.

A wide variety of cobalt(II) complexes are known to bind dioxygen more or less reversibly and are therefore frequently studied as model compounds for natural oxygen carriers and for their use in O_2 storage, as well as in organic synthesis due to their catalytic properties under mild conditions [3]. In this respect, Co(II) complexes with N-donor ligands containing binding units suitable either for the coordination of a single metal ion or for assembling dimetallic centres have been shown to be particularly useful [4]. The catechol oxidases (EC 1.10.3.1) are type 3 copper enzymes containing a dinuclear copper centre [5]. Well-known representatives of these type 3 copper proteins are hemocyanin [6,7], the dioxygen carrier for arthropods and mollusks, and tyrosinase [8]. Catechol oxidase belongs, like tyrosinase, to the polyphenol oxidases which oxidize phenolic compounds to the corresponding quinones in the presence of oxygen. Whereas tyrosinase (EC 1.14.18.1) catalyzes the hydroxylation of tyrosine to dopa (cresolase activity) and the

* Corresponding author. Tel.: +90 344 2191093; fax: +90 344 2191042.
E-mail address: mtumer@ksu.edu.tr (M. Tümer).

1386-1425/$ – see front matter © 2006 Elsevier B.V. All rights reserved.
doi:10.1016/j.saa.2006.09.009

oxidation of dopa to dopaquinone (catecholase activity) with electron transfer to dioxygen, catechol oxidase exclusively catalyzes the oxidation of catechols to quinones without acting on tyrosine [9].

Numerous electrochemical studies have been made for a fairly large number of acyclic and macrocyclic copper(II) complexes derived from Schiff bases. These investigations revealed that the redox properties of copper(II) complexes are markedly influenced by structural and electronic factors [10,11].

The present study deals with the synthesis, characterization, antimicrobial activity, catalyses, thermal and electrochemical properties of the Schiff bases and their metal complexes.

2. Experimental

2.1. Material

All organic compounds and the solvents were purchased from Fluka and Merck. The metal salts $CuCl_2{\cdot}2H_2O$, $CoCl_2{\cdot}6H_2O$, $CdCl_2{\cdot}2H_2O$, $NiCl_2{\cdot}6H_2O$, $SnCl_2{\cdot}2H_2O$ and $ZnCl_2$ were obtained from Fluka and used for complex preparation. 4-Methyl-2,6-di-formylphenol and 4-*t*-butyl-2,6-di-formylphenol were obtained according to the literature method [12].

2.2. Instrumentation

Elemental analyses (C, H, N) were performed using a Carlo Erba 1106 elemental analyser. Infrared spectra were obtained using KBr discs (4000–400 cm^{-1}) on a Shimadzu 8300 FT-IR spectrophotometer. The electronic spectra in the 200–900 nm range were obtained on a Shimadzu UV-160 A spectrophotometer. Magnetic measurements were carried out by the Gouy method using $Hg[Co(SCN)_4]$ as calibrant. Molar conductances of the Schiff base ligands and their transition metal complexes were determined in MeOH ($\sim 10^{-3}$ M) at room temperature using a Jenway Model 4070 conductivity meter. Mass spectra of the ligands were recorded on a VG ZabSpec GC–MS spectrophotometer with fast atom bombardment. ^1H and ^{13}C NMR spectra were recorded on a Varian Gemini XL-200 instrument. TMS was used as internal standard and deuteriated $CDCl_3$ as solvent. The metal contents of the complexes were determined according to the literature methods [13]. Chlorine was determined gravimetrically as silver chloride. The thermal analyses studies of the complexes were performed on a Perkin-Elmer Pyris Diamond DTA/TG Thermal System under nitrogen atmosphere at a heating rate of 10 °C/min.

Catalysis experiments were monitored on a Shimadzu 160-A UV–vis spectrophotometer. The change in the concentration of the TTBD was monitored by optical spectroscopy. For the catalytic activity of the mono- and binuclear complexes Co(II) and the $[Cu(H_2L)]Cl_2$ complex, a similar procedure was adopted for reactions with the aa, the d–d band being monitoring.

2.3. Synthesis of the 2-(2-aminoethyliminomethyl)phenol (H_3A)

The precursor was prepared according to the modified method described earlier [14,15] by mono condensation of the appropriate diamine, with aldehydes. To the vigorously stirred and cool dilute solution ($T = 5$–10 °C) of the ethylenediamine (20 mmol) in the absolute ethanol (100 mL) under argon, was added dropwise a cooled solution of the salicylaldehde (15 mmol) in the absolute ethanol (80 mL). After the addition was complete, the mixture was stirred for 15–30 min and then refluxed for 15–60 min. The resulting solution was evaporated under vacuum to remove the solvent and excess diamine was extracted by benzene and was used for the next step without further purification.

H_3A: Yield (40%), color: yellow, m.p. 105 °C. Found (% calc.): C: 65.80 (65.83), H: 7.40 (7.37), N: 17.10 (17.06). UV–vis: (λ_{max}, nm, EtOH as solvent): 407, 342, 315, 290, 268, 255. i.r.: (KBr, cm^{-1}): 3377 [ν(OH)], 2872 [$\nu(CH_2)$], 2640 [ν(O–H···N)], 1633 [ν(CH=N)], 1377 [ν(C–OH)]. ^1H NMR: ($CDCl_3$ as solvent, δ in ppm): 10.5(s, OH), 6.66–7.99(Ar–H, M), 8.68(CH=N), 4.52(t, NH_2), 3.22; 3.23(t, CH_2, p, CH_2).

2.4. Synthesis of the Schiff bases H_2L, H_3L^1 and H_3L^2

The unsymmetrical Schiff bases were obtained by condensation of the half units and the appropriate aldehydes. To the stirred solution of the precursor (half unit, H_3A) in anhydrous ethanol was added a solution of phtaldialdehyde, 4-methyl-2,6-di-formylphenol and 4-*t*-butyl-2,6-di-formylphenol in anhydrous ethanol. The mixture was concentrated in vacuum by evaporation of the solvent until a colored solid precipitated. The product was filtered, washed with cold solvent and recrystallized from the appropriate solvents (methanol/hexane mixture (1:1) for H_2L, H_3L^1 and H_3L^2) to give colored crystals. General formulae of the ligands are shown in Fig. 1.

The spectral data of the ligands are given below:

H_3L^1: λ_{max}(nm), hexane: 362, 322, 298, 249; toluene: 476, 364, 350, 324; EtOH: 461, 411, 368, 350, 319, 258, 252; MeOH: 407, 365, 315, 286, 280, 253. FT-IR (cm^{-1}, KBr): ν(OH) 3422, $\nu(CH_3)$ 2945, ν(O–H···N) 2741, $\nu(CH{=}N)^x$ 1634, $\nu(CH{=}N)^y$.
H_3L^2: λ_{max}(nm), hexane: 363, 324, 318, 256; toluene: 438, 367, 362, 324; EtOH: 431, 414, 349, 309, 274, 285, 253; MeOH: 424, 362, 318, 280, 254. FT-IR (cm^{-1}, KBr): ν(OH) 3420, $\nu(CH_3)$ 2959, ν(O–H···N) 2590, $\nu(CH{=}N)^x$ 1633, $\nu(CH{=}N)^y$ 1612.
H_2L: λ_{max}(nm), hexane: 389, 350, 334, 274, 259; toluene: 462, 450, 395, 350, 334, 286; EtOH: 431, 414, 349, 309, 274, 285, 253; MeOH: 410, 349, 332, 295, 277. FT-IR (cm^{-1}, KBr): ν(OH) 3370, $\nu(CH_3)$ 2948, ν(O–H···N) 2590, $\nu(CH{=}N)^x$ 1631, $\nu(CH{=}N)^y$ 1620.
x and y are salicylidene and diformyl fragments, respectively.

2.5. Preparation of the complexes

The complexes were prepared by similar methods. A solution of the metal salt (1 mmol for the ligand H_2L, 2 mmol for the ligands H_3L^1 and H_3L^2) in the absolute MeOH (25 mL) was added to a solution of the ligands H_2L, H_3L^1 and H_3L^2 (1 mmol) in the absolute MeOH (20 mL) and the mixture was boiled under reflux for 6–7 h. At the end of the reaction, determined by t.l.c., the precipitate was filtered off, washed with EtOH and Et_2O, and dried in vacuo.

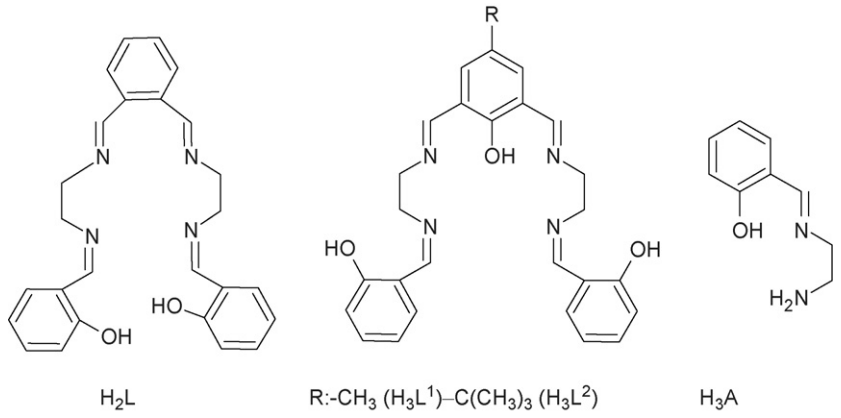

Fig. 1. General formulae of the ligands H_3A, H_2L, H_3L^1 and H_3L^2.

$Cd_2(L^1)Cl$: λ_{max}(nm), EtOH: 361, 281, 221. Λ (Ω^{-1} cm^2 mol^{-1}): 17.2. FT-IR (cm^{-1}, KBr): $\nu(CH_3)$ 2948, $\nu(CH_2)$ 2904, $\nu(CH{=}N)^x$ 1610, $\nu(CH{=}N)^y$ 1590, ν(M–O) 532, ν(M–N) 434. $Cu_2(L^1)Cl$: λ_{max}(nm), EtOH: 612, 581, 361, 281, 221. Λ (Ω^{-1} cm^2 mol^{-1}): 18.9. FT-IR (cm^{-1}, KBr): $\nu(CH_3)$ 2947, $\nu(CH_2)$ 2897, $\nu(CH{=}N)^x$ 1620, $\nu(CH{=}N)^y$ 1595, ν(M–O) 503, ν(M–N) 444. μ_{eff} (B.M.): 1.10. $Co_2(L^1)Cl$: λ_{max}(nm), EtOH: 652, 468, 390, 350, 335, 280, 256. Λ (Ω^{-1} cm^2 mol^{-1}): 16.5. FT-IR (cm^{-1}, KBr): $\nu(CH_3)$ 2926, $\nu(CH_2)$ 2896, $\nu(CH{=}N)^x$ 1641, $\nu(CH{=}N)^y$ 1600, ν(M–O) 473, ν(M–N) 444. μ_{eff} (B.M.): 4.18. $Ni_2(L^1)Cl$: λ_{max}(nm), EtOH: 557, 393, 345, 317, 240. Λ (Ω^{-1} cm^2 mol^{-1}): 17.0. FT-IR (cm^{-1}, KBr): $\nu(CH_3)$ 2926, $\nu(CH_2)$ 2900, $\nu(CH{=}N)^x$ 1625, $\nu(CH{=}N)^y$ 1604, ν(M–O) 543, ν(M–N) 471. $Sn_2(L^1)Cl$: λ_{max}(nm), EtOH: 364, 352, 345, 301, 241. Λ (Ω^{-1} cm^2 mol^{-1}): 18.3. FT-IR (cm^{-1}, KBr): $\nu(CH_3)$ 2997, $\nu(CH_2)$ 2930, $\nu(CH{=}N)^x$ 1623, $\nu(CH{=}N)^y$ 1595, ν(M–O) 510, ν(M–N) 475. $Zn_2(L^1)Cl$: λ_{max}(nm), EtOH: 471, 348, 275, 255. Λ (Ω^{-1} cm^2 mol^{-1}): 15.9. FT-IR (cm^{-1}, KBr): $\nu(CH_3)$ 2922, $\nu(CH_2)$ 2900, $\nu(CH{=}N)^x$ 1639, $\nu(CH{=}N)^y$ 1605, ν(M–O) 497, ν(M–N) 467.

$Cd_2(L^2)Cl$: λ_{max}(nm), EtOH: 383, 324, 303, 256. Λ (Ω^{-1} cm^2 mol^{-1}): 18.4. FT-IR (cm^{-1}, KBr): $\nu(CH_3)$ 2905, $\nu(CH_2)$ 2874, $\nu(CH{=}N)^x$ 1605, $\nu(CH{=}N)^y$ 1605, ν(M–O) 563, ν(M–N) 428. $Cu_2(L^2)Cl$: λ_{max}(nm), EtOH: 562, 549, 359, 28, 220. Λ (Ω^{-1} cm^2 mol^{-1}): 16.8. FT-IR (cm^{-1}, KBr): $\nu(CH_3)$ 2955, $\nu(CH_2)$ 2898, $\nu(CH{=}N)^x$ 1613, $\nu(CH{=}N)^y$ 1604, ν(M–O) 562, ν(M–N) 444. μ_{eff} (B.M.): 1.11. $Co_2(L^2)Cl$: λ_{max}(nm), EtOH: 655, 430, 391, 352, 331, 293, 255. Λ (Ω^{-1} cm^2 mol^{-1}): 17.2. FT-IR (cm^{-1}, KBr): $\nu(CH_3)$ 2961, $\nu(CH_2)$ 2900, $\nu(CH{=}N)^x$ 1643, $\nu(CH{=}N)^y$ 1600, ν(M–O) 532, ν(M–N) 475. μ_{eff} (B.M.): 4.15. $Ni_2(L^2)Cl$: λ_{max}(nm), EtOH: 565, 450, 392, 345, 321, 255. Λ (Ω^{-1} cm^2 mol^{-1}): 17.3. FT-IR (cm^{-1}, KBr): $\nu(CH_3)$ 2961, $\nu(CH_2)$ 2904, $\nu(CH{=}N)^x$ 1627, $\nu(CH{=}N)^y$ 1594, ν(M–O) 536, ν(M–N) 470. $Sn_2(L^2)Cl$: λ_{max}(nm), EtOH: 446, 359, 329, 294, 289, 231. Λ (Ω^{-1} cm^2 mol^{-1}): 15.9. FT-IR (cm^{-1}, KBr): $\nu(CH_3)$ 2995, $\nu(CH_2)$ 2960, $\nu(CH{=}N)^x$ 1610, $\nu(CH{=}N)^y$ 1590, ν(M–O) 514, ν(M–N) 460. $Zn_2(L^2)Cl$: λ_{max}(nm), EtOH: 426, 350, 338, 276. Λ (Ω^{-1} cm^2 mol^{-1}): 18.1. FT-IR (cm^{-1}, KBr): $\nu(CH_3)$ 2986, $\nu(CH_2)$ 2957, $\nu(CH{=}N)^x$ 1627, $\nu(CH{=}N)^y$ 1597, ν(M–O) 529, ν(M–N) 432.

$[Cd(H_2L)]Cl_2$: λ_{max}(nm), EtOH: 422, 358, 263. Λ (Ω^{-1} cm^2 mol^{-1}): 57.7. FT-IR (cm^{-1}, KBr): ν(OH) 3372, $\nu(CH_2)$ 2904, $\nu(CH{=}N)^x$ 1614, $\nu(CH{=}N)^y$ 1597, ν(M–O) 532, ν(M–N) 434. $[Cu(H_2L)]Cl_2$: λ_{max}(nm), EtOH: 613, 377, 284, 250. Λ (Ω^{-1} cm^2 mol^{-1}): 61.3. FT-IR (cm^{-1}, KBr): ν(OH) 3370, $\nu(CH_2)$ 2900, $\nu(CH{=}N)^x$ 1618, $\nu(CH{=}N)^y$ 1600, ν(M–O) 534, ν(M–N) 442. μ_{eff} (B.M.): 1.79. $[Co(H_2L)]Cl_2$: λ_{max}(nm), EtOH: 643, 382, 291, 248. Λ (Ω^{-1} cm^2 mol^{-1}): 60.4. FT-IR (cm^{-1}, KBr): ν(OH) 3372, $\nu(CH_2)$ 2893, $\nu(CH{=}N)^x$ 1620, $\nu(CH{=}N)^y$ 1598, ν(M–O) 490, ν(M–N) 468. μ_{eff} (B.M.): 4.27. $[Ni(H_2L)]Cl_2$: λ_{max}(nm), EtOH: 610, 376, 288, 254. Λ (Ω^{-1} cm^2 mol^{-1}): 58.9. FT-IR (cm^{-1}, KBr): ν(OH) 3375, $\nu(CH_2)$ 2907, $\nu(CH{=}N)^x$ 1608, $\nu(CH{=}N)^y$ 1600, ν(M–O) 518, ν(M–N) 475. $[Sn(H_2L)]Cl_2$: λ_{max}(nm), EtOH: 432, 390, 278, 260. Λ (Ω^{-1} cm^2 mol^{-1}): 54.6. FT-IR (cm^{-1}, KBr): ν(OH) 3370, $\nu(CH_2)$ 2908, $\nu(CH{=}N)^x$ 1615, $\nu(CH{=}N)^y$ 1594, ν(M–O) 507, ν(M–N) 470. $[Zn(H_2L)]Cl_2$: λ_{max}(nm), EtOH: 398, 373, 260, 245. Λ (Ω^{-1} cm^2 mol^{-1}): 57.1. FT-IR (cm^{-1}, KBr): ν(OH) 3372, $\nu(CH_2)$ 2905, $\nu(CH{=}N)^x$ 1625, $\nu(CH{=}N)^y$ 1598, ν(M–O) 507, ν(M–N) 450.

2.6. Catalytic oxidation of 2,6-di-tert-butylphenol

In a dichloromethane/methanol solvent mixture (1:1, 50 mL), the Co(II) and Cu(II) complexes were dissolved. To it 2,6-di-*tert*-butylphenol was added and the solution was stirred for 48–60 h. The solution was then filtered and the filtrate was evaporated to dryness. The 5 mL of methanol were added to dissolve the excess 2,6-di-*tert*-butylphenol.

For measuring the progress of the reaction, 50 μL from the aliquot was passed through an Amberlyst cationic ion-exchanger and washed with 10 mL (2 × 5) dichloromethane. The change in the concentration of product 3,3′-5,5′-tetra-*tert*-butyl-4,4′-diphenoquinone (TTBD) was monitored by optical spectroscopy.

2.7. Catecolase activity studies

The reaction of the Co(II) complexes and the $[Cu(H_2L)]Cl_2$ complex with 3,5-di-*tert*-butylcatechol (3,5-DTBC) and ascorbic acid (aa) was monitored as follows: in a typical exper-

iment, 100 mm^3 of a solution of the complex in methanol ([C]o = 2.4×10^{-5} mol dm^{-3}) was added to a 1 cm path length cell containing 3 cm^3 of O_2-saturated methanol at 25 °C. The reaction was initiated by the addition of 100 cm^3 of catechol solution ([3,5-DTBC]o = 1.0×10^{-3} to 1.0×10^{-4} mol dm^{-3}). In a separate set of experiments, the kinetic determinations were performed without the catalyst. The UV–vis spectra of the original solution, of the solution directly after the addition and after 5, 10, 15 and 20 min were recorded and corrected for volume changes.

2.8. Electrochemical experiments

Electrochemical studies were carried out with a BAS 100B/W Electrochemical Workstation equipped with a low current module (BAS PA-1) at a platinum disk electrode (area 0.68 cm^2). Cyclic voltammetric measurements were made at room temperature in a single compartment cell (BAS model C-3 cell stand) with a platinum counter electrode and an Ag/Ag^+ reference electrode (BAS). All potentials are reported with respect to Ag/Ag^+.

The tetrabutylammonium perchlorate ($TBAClO_4$) as a supporting electrolyte was used as received. Acetonitrile (MeCN) was purified by drying with calcium hydride, followed by distillation from phosphorus pentoxide. It was kept over molecular sieves (3 Å Merck) in order to eliminate its water content as much as possible. The solutions for electrochemical measurements contained 3×10^{-3} M complex in 0.1 M $TBAClO_4$/MeCN. The solutions were deoxygenated by passing dry nitrogen through the solution for 30 min prior to the experiments, and during the experiments the flow was maintained over the solution.

2.9. Preparation of microorganism cultures

The growth inhibitory activity of the chemical matter was tested against thirteen bacteria [*Corynebacterium xerosis* UC 9165, *Bacillus brevis* NRS, *Bacillus megaterium* DSM 32, *Bacillus cereus* EU, *Mycobacterium smegmatis* CCM 2067, *Staphylococcus aureus* Cowan 1, *Pseudomonas aeruginosa* ATCC 27853, *Klebsiella pneumoniae* FMC 5, *Enterococcus faecalis* ATTC 15753, *Micrococcus luteus* LA 2971, *Yersinia enterocolitica* CMC 120 and *Escherichia coli* DM] and three yeasts [*Kluvyeromyces fragilis* A 230, *Saccharomyces cerevisiae* WET 136 and *Candida albicans* ATCC 1023]. The antimicrobial activities of the ligands and their metal complexes were determined using the agar-disc diffusion method as will be described below. The bacteria were first incubated at 37 ± 0.1 °C for 24 h in nutrient broth (Difco), and the yeasts were incubated in sabouraud dextrose broth (Difco) at 25 ± 0.1 °C for 24 h. The cultures of the bacteria and yeast were injected into the petri dishes (9 cm) in the amount of 0.1 mL. And then, mueller hinton agar and sabouraud dextrose agar (sterilized in a flask and cooled to 45–50 °C) were homogenously distributed onto the sterilized petri dishes in the amount of 15 mL. Subsequently, the sterilized blank paper discs of 6 mm diameter were saturated with 1200 μg of the ligands and their metal complexes per disc. The discs thus treated were placed onto the agar plates, which had previously been inoculated with the above organisms. In addition, blank paper discs treated with ampicillin, streptomycin and nystatin-saturated antibiotics were used as positive controls. Afterwards the plates combined with the discs were left at 4 °C for 2 h, the plates injected with yeast were incubated at 25 ± 0.1 °C for 24 h, and ones injected with bacteria were incubated at 37 ± 0.1 °C for 24 h. After 24 h, inhibition zones appearing around the discs were measured and recorded in mm. The initial number of microorganisms in the suspension was determined for the total yeasts and bacterial count during 24 h at 37 °C for bacteria and 48 h 25 °C for yeasts [16,17].

3. Results and discussion

Analytical data of the ligands and their complexes are given in Table 1 and are in well agreement with the expected values. To prepare the ligands H_2L, H_3L^1 and H_3L^2, firstly, we prepared the starting material 2-(2-aminoethyliminomethyl)phenol (H_3A). One of a major difficulties in obtaining the Schiff base H_3A is due to its bis product formation. Other problem is low yield of the compound H_3A. The compound 2-(2-aminoethylimino-methyl)phenol (H_3A) is prepared from salicylaldehyde and ethylenediamine in a 1:1 molar ratio in an ethanolic solution, with subsequent removal of the excess diamine with extraction into benzene. The reaction has been carried out using highly dilute conditions. The reaction product has not been crystallized. Because, both bis product [2-[({2-[(2-hydroxybenzylidene)amino]ethyl}imino)methyl]phenol] and the half unit compound H_3A soluble in the common organic solvents. Moreover, as the bis product has not free primary amine group, it does not react with carbonyl compounds. But, the starting material H_3A has the free $–NH_2$ functional group. This free $–NH_2$ group may easily react with carbonyl compounds as the amines. Therefore, this starting material, immediately, has been used without further purification. Also, its spectroscopic and analytical data confirm the resulting of the compound H_3A. To prepare the ligands H_2L, H_3L^1 and H_3L^2, the carbonyl compounds phtaldialdehyde, 4-methyl-2,6-di-formylphenol and 4-*t*-butyl-2,6-di-formyl-phenol with the amine compound H_3A have been used in 1:2 molar ratio (carbonyl:amine) in ethanolic solution. Condensation between aldehydes and amines is realized in different reaction conditions, and in different solvents. In this study, ethanol, at room temperature or in refluxing conditions, is also a valuable solvent for the preparation of Schiff bases. Degradation of the Schiff bases can occur during the purification step. Chromatography of Schiff bases on silica gel can cause some degree of decomposition of the Schiff bases, through hydrolysis. In this case, it is better to purify the Schiff base by crystallization. If the Schiff bases are insoluble in hexane or cyclohexane, they can be purified by stirring the crude reaction mixture in these solvents, sometimes adding a small portion of a more polar solvent (Et_2O, CH_2Cl_2), in order to eliminate impurities. In general, Schiff bases are stable solids and can be stored without precautions. Condensation of salicylaldehydes or salicylaldehyde derivatives with 1,2-diamines leads to the formation of one extremely important class of ligands, generally known as “Salens”. Salicylaldehydes

Table 1
Analytical and physical data for the Schiff Base ligands and their Cu(II) and Cd(II) complexes

Compound	Color	Yield (%)	m.p. (°C)	Found (calculated) (%)		*N*	*M*
				C	H		
H_3L^1	Light brown	85	115	71.07 (71.03)	6.23 (6.18)	12.31 (12.27)	–
$[Cu_2(L^1)]Cl$	Brown	72	>250	52.65 (52.63)	4.04 (4.06)	9.12 (9.09)	20.71 (20.64)
$[Cd_2(L^1)]Cl$	Brown	65	>250	45.46 (45.42)	3.54 (3.51)	7.88 (7.85)	31.57 (31.52)
$[Co_2(L^1)]Cl$	Black	71	>250	53.44 (53.43)	4.14 (4.12)	9.21 (9.24)	19.48 (19.43)
$[Ni_2(L^1)]Cl$	Dark red	68	>250	53.49 (53.46)	4.10 (4.12)	9.28 (9.24)	19.47 (19.38)
$[Zn_2(L^1)]Cl$	Light red	70	>250	55.35 (55.32)	4.07 (4.04)	9.01 (9.04)	21.19 (21.12)
$[Sn_2(L^1)]Cl$	Red	75	>250	44.60 (44.63)	3.46 (3.44)	7.74 (7.71)	32.74 (32.70)
H_3L^2	Yellow	80	97	72.22 (72.27)	6.90 (6.87)	11.30 (11.24)	–
$[Cu_2(L^2)]Cl$	Brown	71	>250	54.78 (54.75)	4.69 (4.71)	8.55 (8.52)	19.40 (19.33)
$[Cd_2(L^2)]Cl$	Brown	68	>250	47.71 (47.67)	4.16 (4.13)	7.46 (7.41)	29.81 (29.76)
$[Co_2(L^2)]Cl$	Black	74	>250	55.54 (55.52)	4.76 (4.78)	8.67 (8.64)	18.25 (18.18)
$[Ni_2(L^2)]Cl$	Light red	77	>250	55.56 (55.55)	4.77 (4.78)	8.66 (8.64)	18.20 (18.13)
$[Zn_2(L^2)]Cl$	Yellow	65	>250	54.47 (54.44)	4.72 (4.69)	8.50 (8.47)	19.84 (19.77)
$[Sn_2(L^2)]Cl$	Yellow	68	>250	47.93 (46.88)	4.08 (4.04)	7.27 (7.30)	30.99 (30.92)
H_2L	Red orange	90	72–74	73.29 (73.26)	6.15 (6.10)	13.18 (13.15)	–
$[Cu(H_2L)]Cl_2$	Black	73	>250	55.71 (55.66)	4.69 (4.64)	10.03 (9.99)	12.71 (12.66)
$[Cd(H_2L)]Cl_2$	Orange	70	>250	51.25 (51.20)	4.22 (4.27)	9.15 (9.19)	11.70 (11.65)
$[Co(H_2L)]Cl_2$	Black	72	>250	55.54 (55.52)	4.76 (4.78)	8.67 (8.64)	18.25 (18.18)
$[Ni(H_2L)]Cl_2$	Green	69	>250	55.56 (55.55)	4.77 (4.78)	8.66 (8.64)	18.20 (18.13)
$[Zn(H_2L)]Cl_2$	Yellow	70	>250	54.47 (54.44)	4.72 (4.69)	8.50 (8.47)	19.84 (19.77)
$[Sn(H_2L)]Cl_2$	Orange	75	>250	47.93 (46.88)	4.08 (4.04)	7.27 (7.30)	30.99 (30.92)

bearing different substituents are obtained by the introduction of a formyl group, using a simple and well established reaction, into the corresponding phenol derivatives (Fig. 1). The Schiff base ligands obtained from the condensation reactions soluble in polar organic solvents such as, EtOH, MeOH, $CHCl_3$, $(C_2H_5)O$, etc.

In the case of the ligands and their metal complexes, it is particularly important to establish whether the molecules retain the imine character of their phenol precursor. The most useful techniques to investigate the tautomeric forms of these ligands are UV and NMR spectroscopy, while IR seems of limited value here because location of the ν(C=O) and ν(C–O) stretches in the spectra is obscured by the abundance of aromatic skeletal modes. In case of Schiff bases calculations of related forms of proton transfer (pt) tautomer are possible because pt stationary states are formed. Tautomeric forms of the polydentate ligands H_3L^1 and H_3L^2 are shown in Fig. 2. In order to investigate the keto-enol tautomeric forms of the free ligands, the electronic spectra were measured in heptane, chloroform, toluene and ethanol. The UV spectral data of the ligands are given in Section 2.

The stronger solute/solvent hydrogen bonding by the hydroxyl or azomethine groups, as well as the increasing importance of the solvent polarity/polarizability in the stabilization of the electronic excited state lead to a hypsochromic shift with both increasing solvent hydrogen bond acceptor basicity and solvent polarity/polarizability. This suggests that most of the solvatochromism in the ligands is due to the solvent polarity and basicity rather than to the solvent acidity. As the number of CH_2 groups in ROH increases, the dielectric constant decreases. If the molecules contain a polar component (OH) and a non-polar component (R), then the polarity of a compound reflects the balance between these two components. As the relative amount of hydrocarbon character increases, the polarity decreases. Note that hexane, which is 100% hydrocarbon, is the least polar solvent. For example, in hexane and toluene, the ligand H_3L^1 shows eight bands in the 476–249 nm range. However, in ethanol and methanol, the ligand H_3L^1 has the bands in the 461–252 nm range. In non-polar solvents, the bands observed in the 476–322 nm range may be assigned to the ketoamine tautomer and the latter to the enolimine tautomer of the Schiff base ligands [18]. However, in polar solvents, the bands at approximately the same region can be attributed to the enolimine tautomeric forms. In the toluene and hexane solvents, the free ligands have the ketoamine form. However, in EtOH and $CHCl_3$ solvents, the enol-imine forms have been observed [19]. Other ligands have also electronic transitions in polar and non-polar solvents.

Electronic spectra of the ligands and their metal complexes have been measured in EtOH and the numerical data are given in Section 2. All the complexes show an intense band in the 324–303 nm range which is assigned to a π–π^* transition associated with the azomethine linkage [20]. The spectra of the complexes show intense bands in the high-energy region in the 487–358 nm range which can be assigned to charge transfer L → M bands [21]. The bands observed in the 628–549 nm region can be attributed to d–d transitions of the metal ions. In the spectra of the Cu(II) complexes, the d–d transitions are observed in the 628–549 nm range. These values are of particular importance since they were highly dependent on the geometry of the molecule. It is known that the transitions from a square-planar structure to a deformed tetrahedral structure leads to a red shift of absorption in the electronic spectra [22]. Thus, the smaller value of the wavelength of the band corresponding to the transitions is resemblance between the geometry of the complex and that of square-planar complex.

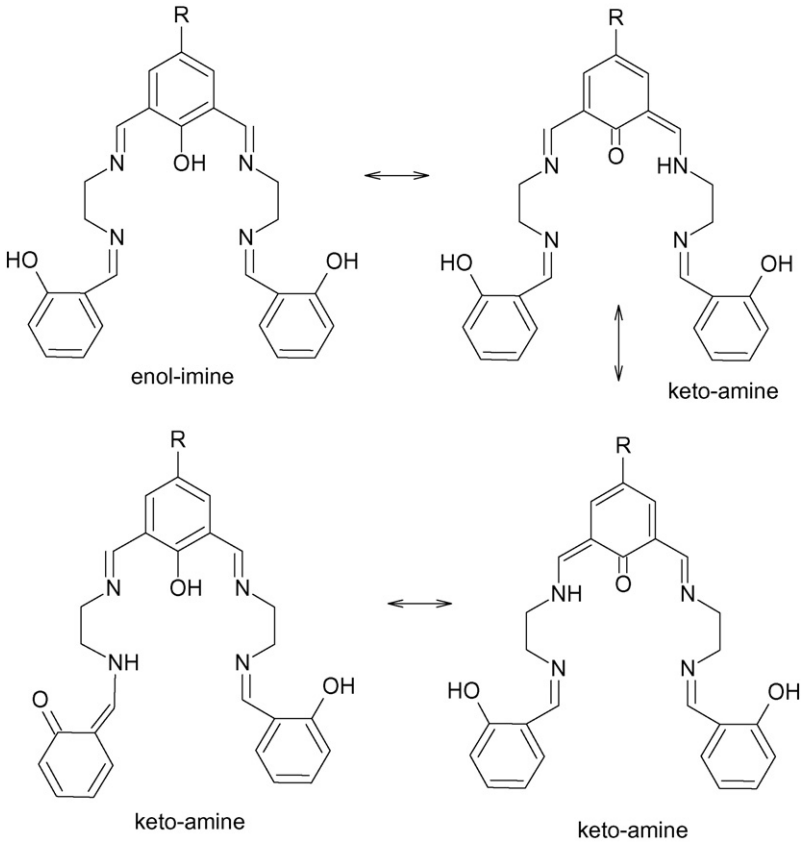

Fig. 2. Tautomeric forms of the Schiff base ligands in the organic solvents.

IR data of the ligands and their complexes are given in Section 2. In the spectra of the starting compound H_3A with the final compounds $H_3L^1$and H_3L^2, the broad bands in the 3370–3422 cm^{-1} range can be attributed to the ν(OH) cm^{-1} vibration. In the transition metal complexes, the bands due to the OH modes are no longer observed, denoting that all the hydroxyl protons are displaced by M^{II} ions (Cd, Cu, Co, Ni, Sn and Zn) leading to covalent ν(M–O) bonding with the ligands. In the ligands, the broad bands in the 2741 and 2590 cm^{-1} comes from the intramolecular hydrogen bonding along the fenolic –OH and azomethine –CH=N– groups, these bands are disappear as complexation between the oxygen and nitrogen atoms with metals ions. The ν(CH=N) band (1634–1605 cm^{-1}) is shifted to the lower wave numbers denoting that the nitrogen atom of the azomethine group is coordinated to the metal(II) ions. The bonding of the metal(II) ions to the ligands through the nitrogen and oxygen atoms is further supported by the presence of new bands in the 563–473 and 475–428 cm^{-1} range due to the ν(M–O) and ν(M–N), respectively.

The molar conductances data of the ligands and their complexes are listed in Section 2. Conductance measurements were carried out in EtOH using 10^{-3} M solutions. Equivalent conductance of the complexes of the ligand H_2L were found in the range 54.6–61.3 Ω^{-1} cm^2 mol^{-1} suggesting that the complexes belong to 1:2 electrolytes [23]. Two chloride ions are outside the coordination sphere. That is, they do not coordinate to the metal ion. The equivalent conductance of the binuclear complexes of the ligands H_3L^1 and H_3L^2 were found to be in the range 15.9–18.9 Ω^{-1} cm^2 mol^{-1} suggesting that the complexes belong to the 1:1 electrolytes. This indicates that the chloride ion in the complexes is not coordinated to the metal ions.

The magnetic moments (as B.M.) of the complexes were measured at room temperature and data are given in Section 2. The Cd(II), Sn(II) and Zn(II) complexes of the ligands have the diamagnetic character. Analytical and spectroscopic evidences show that the metal ions Cd(II), Sn(II) and Zn(II) have four coordinations. Therefore, we can suggest that the geometry around the metal centres for these metal ions is the tetrahedral. The room temperature magnetic moment measurements show that the nickel–Schiff base complexes, are diamagnetic, suggesting low-spin (dsp^2) square-planar geometries as expected for the d^8 system. The electronic absorption spectra of all nickel(II) complexes display two spin-allowed d–d transitions corresponding to electronic excitation from the three lower levels to the empty d_{x2-y2} orbital in the square-planar geometry of nickel(II) complexes with a Ni_2–N_4O_3 chromophore. In addition to the spin-allowed d–d transitions, the spectra are characterized by strong absorption bands within the 393 and 392 nm which can be attributed to intramolecular charge transfer (CT) interactions and to π–π^* internal ligand transitions. All cobalt(II) complexes of the ligands H_2L, H_3L^1 and H_3L^2 have magnetic moments values in the 4.20, 4.19 and 4.27 B.M. range, and these values are consistent with the tetrahedral geometry [24].

In the binuclear complexes, the magnetic susceptibility studies measured at room temperature (298 K) are substantially lower than the spin only value of 1.73 B.M., which may be due to the presence of antiferromagnetic coupling. Room temperature susceptibilities gave μ_{eff} values at the 1.10 and 1.11 B.M. for the complexes $[Cu_2(L^1)]Cl$ and $[Cu_2(L^1)]Cl$, respectively. The reason for such an observation is due to the quenching of the unpaired spin of the metal ion by the unpaired spin on the adjacent Cu(II) ion, coupled by superexchange interaction (Cu–O–Cu). In other words, the complex $[Cu(L)]_2Cl$ has a magnetic moment value (1.79 B.M.) and this indicates that the geometry around the Cu(II) ion is tetrahedral. The coordination geometry in the Co(II) dimers is most likely distorted tetrahedral, as suggested by the observed room temperature μ_{eff} values per Co atom (4.2–4.5 μ_B), in the range reported for several tetrahedral Schiff bases Co(II) complexes [25].

The formulation of the ligands are deduced from analytical data, ^1H and ^{13}C NMR and further supported by mass spectroscopy. The relatively low intensities of the molecular ion peaks, $[M]^+$, are indicative of the ease of fragmentation of the compounds, and this may reflect the number of heteroatoms present in each structure. The spectra of the ligands H_2L, H_3L^1 and H_3L^2 show peaks at *m/e* 426, 455 and 497, respectively. These peaks can attributed to the molecular ion peaks $[M]^+$. All the ligands decompose in a similar way. In the spectra of the ligands, the highest intensity peaks are at *m/e* 144 (100%), 160 (100%) and 202 (100%). They may be assigned to the $[C_8H_6N_2O]^{2+}$, $[C_9H_8N_2O]^{2+}$ and $[C_{12}H_{14}N_2O]^{2+}$ ions which are formed by the loss of other parts (salicylidene moiety together with daimine fragment) of the molecular ions.

The ^1H and ^{13}C NMR spectra of the ligands were recorded in $CDCl_3$ and data are given in Table 2. The ligands have two different surroundings. These are the alkylformylphenol and salicylidene moiety. The chemical shifts of these are different. In two ligands, there are two azomethine groups in the different centres. In addition, there are methylene chains as bridge. In the methylene chain, there are two CH_2 groups as α-CH_2 and α'-CH_2. These are shown in the different regions. The ligands show approximately the same peaks. In the ^1H NMR spectrum, the triplets in the 1.26–1.18 ppm range can be attributed to the protons of the α-CH_2 and α'-CH_2 groups. The protons of the methyl group of the aromatic ring are observed at 2.29 ppm as a singlet. The multiplets in the 6.62–7.33 ppm range may be assigned to the protons of benzene rings. The azomethine protons of the ligand are observed in the 8.36 and 8.42 ppm range as the singlet. A singlet in the 10.45 ppm may be attributed to the OH proton. When D_2O is added to the solution of the ligands, the OH peaks disappear. Other ligand shows also similar spectral properties. In the spectrum of the Cd(II) complex of the H_3L^1 ligand, signals due to the hydrogen atom of the azomethine groups of the ligand shifted to the downfield according to the free ligand. This shows that the nitrogen atom of the azomethine group is coordinated to the metal ions. The OH signals observed for the ligands had disappeared confirming that the phenolic C–OH group is coordinated to the transition metal ions. In the complex, the signals of the methylene groups also shifted to the downfield.

^{13}C NMR spectra of the ligands and their Cd(II) complexes were recorded in $CDCl_3$ and are a good diagnostic tool for determining the mode of bonding. The ^{13}C NMR spectra of the ligands and their complexes demonstrate similar properties. In the spectrum of the ligand H_3L^1, signals due to the azomethine carbon atoms are observed in the 168.48 and 163.05 ppm. In the Cd(II) complex, these signals are shifted downfield, suggesting the involvement of the nitrogen lone pair in coordination with the metal ion. The signals of the carbon atoms of the benzene rings are observed approximately in the 118.95–157.75 ppm range and the signals observed at 61.79 and 62.50 ppm may be attributed to the carbon atoms of the α-CH_2 and α'-CH_2, respectively. The signal at the 21.65 ppm can be attributed to the methyl carbon atom of the benzene ring. However, in the spectra of the Cd(II) complex, the signals due to these groups are observed at the 60.05, 62.21 and 21.12 ppm.

3.1. Catecholase activity

The ability of the complexes to oxidise acid and catechol substrates using molecular oxygen was examined using as substrates aa and 3,5-DTBC. Catalytic studies were performed in methanol solution owing to the good solubility of the complexes as well as the substrate in methanol. The oxidation product 3,5-di-*tert*-butyl-*o*-banzoquinone (3,5-DTBQ) is considerably stable and exhibits a strong absorption at 400 nm. Therefore, the activities and reaction rates can be determined using electronic spectroscopy by following the appearance of the absorption maximum of the quinone. Phenolic compounds have a specific reactivity due to the interaction of the hydroxyl groups and the aromatic ring not found in either the aromatic or hydroxy group alone. This is due to the freedom of two electrons from the oxygen atom being able to partially shift. The phenolic molecule becomes more reactive due to this electron shift. In particular, the withdrawal of electron charge from the oxygen tends

Table 2
The ^1H (^{13}C) NMR data (as ppm) for the Schiff base ligands and their diamagnetic complexes using $CDCl_3$ as solvent

Compound	αCH_2	$\alpha' CH_2$	CH_3	*t*-Bu	Ar	CH=N	OH
H_3L^1	1.26 (61.79)	1.18 (62.50)	2.29 (21.65)	–	6.62–7.33 (118.95–157.75)	8.36 (168.48)	10.45
H_3L^2	1.43 (61.42)	1.41 (61.75)	–	1.20 (33.21)	6.80–7.85 (115.33–158.39)	8.40 (168.47)	10.60
H_2L	1.28 (60.50)	1.30 (61.95)	–	–	6.74–7.65 (112.45–158.38)	8.65 (164.33)	10.55
$Cd_2(L^1)$	1.35 (60.05)	1.24 (62.21)	2.32 (21.12)	–	6.43–7.72 (115.56–159.48)	8.63 (164.92)	–
$Cd_2(L^2)$	1.57 (60.82)	1.58 (59.25)	–	1.37 (32.75)	6.19–7.75 (112.74–159.80)	8.73 (166.76)	–
$[Cd(L^4)]_2Cl$	1.68 (61.77)	1.52 (62.63)	–	–	6.44–7.87 (113.22–156.44)	8.85 (165.80)	10.53

αCH_2 coupling constant $J \sim 6$ Hz, CH_3 coupling constant $J \sim 3$ Hz.

to make the –OH group more likely to form a hydronium ion, thus increasing the acidity of the molecule. The electron shift also leads to more hydrogen bonding possibilities. This hydrogen bonding is what gives the phenolic its ability to bind with proteins *via* the weak hydrogen bonding force. When a phenolic ring has two adjacent hydroxyl groups, it may oxidise to a quinone. Once formed the quinones may also react with electron rich compounds (negative charge). The simplest phenolic compound substrate of polyphenol oxidases is catechol since it has the basic *o*-di-hydroxyphenol structure, yet, this does not mean that it is the best substrate. Any substitution on the ring (position and nature of the substituent) affects the rate of the enzymatic reaction. As an example, the oxidation rate for 3,4-di-hydroxyphenolic compounds was higher than the rate of oxidation for 2,3-di-hydroxyphenolic compounds [26]. The presence of an electron donating group at position 4 increases the rate of the oxidation reaction, whereas an electron withdrawing-group reduces substrate reactivity [27]. The electron-pushing groups make the catalyst more active by increasing the electron density on the imine-nitrogen, which thus positively influences the hydrogen bond-formation with the substrate, as has been proposed in the pre-equilibrium step prior to oxidation (Scheme 1). On the other hand, substitute groups on the benzene ring also decrease the affinity for the enzyme possibly due to steric hindrance [28]. In addition to, there are also other factors that need to be considered, such as electrochemical properties, the geometry imposed by the ligands on the metal ion and the nature of any exogenous donors. While the ligand H_3L^2 has the *tert*-butyl group at para position of the di-formyl ring, the ligand H_3L^1 has the methyl group in the same position. The *tert*-butyl group gives to the ring more electron density than the methyl group. Therefore, the reactivity of the complex increases.

The two-electron oxidation of 3,5-DTBC to quinone was investigated since this is the reaction that the cobalt-containing enzyme catechol oxidase catalyses. In order to compare the difference between mononuclear and dinuclear complexes, we have studied our cobalt complexes for catecholase activity, using the changes in the electronic spectrum after the addition of the 3,5-DTBC substrate. The catecholase activity of the $[Cu(H_2L)]Cl_2$, $[Co(H_2L)]Cl_2$, $[Co_2(L^1)]Cl$ and $[Co_2(L^2)]Cl$ complexes has been studied with the help of electronic spectroscopy by monitoring the appearance of the absorption maximum of the substituted quinone product ($\lambda_{max} = 400$ nm, $\varepsilon_{max} = 1900\ M^{-1}\ cm^{-1}$). In binuclear cobalt(II) complexes, larger magnetic exchange interaction has been observed when the planarity of the metal centre increases. Therefore, binuclear systems with larger magnetic interaction should exhibit greater catalytic activity. The catecholase activity studies of a few of the present complexes reveal that only the complexes of the ligands H_3L^1 and H_3L^2 have significant catalytic activity with respect to the aerial oxidation of 3,5-DTBC to its corresponding quinones compared to complexes of the ligand H_2L. This behavior can be explained by the fact that two cobalt centres must be nearby to link two phenolic oxygen atoms of catechol to mediate the redox reaction. The complex $[Co(H_2L)]Cl_2$ shows little catalytic activity as it is mononuclear. In other words, the complex $[Cu(H_2L)]Cl_2$ does not show the any activity. The Co(II) complexes proved to be significantly more efficient, generally effecting efficient conversion to the *o*-quinone within 24 h and with excellent recyclability. The overall stoichiometry is given by the equation:

$$DBCatH_2 + 0.5O_2 \rightarrow \ DTBQ \ + \ H_2O$$

Suggested catalytic cycle for the 3,5-di-*tert*-butylcatechol by the Co(II) complexes is shown in Scheme 1.

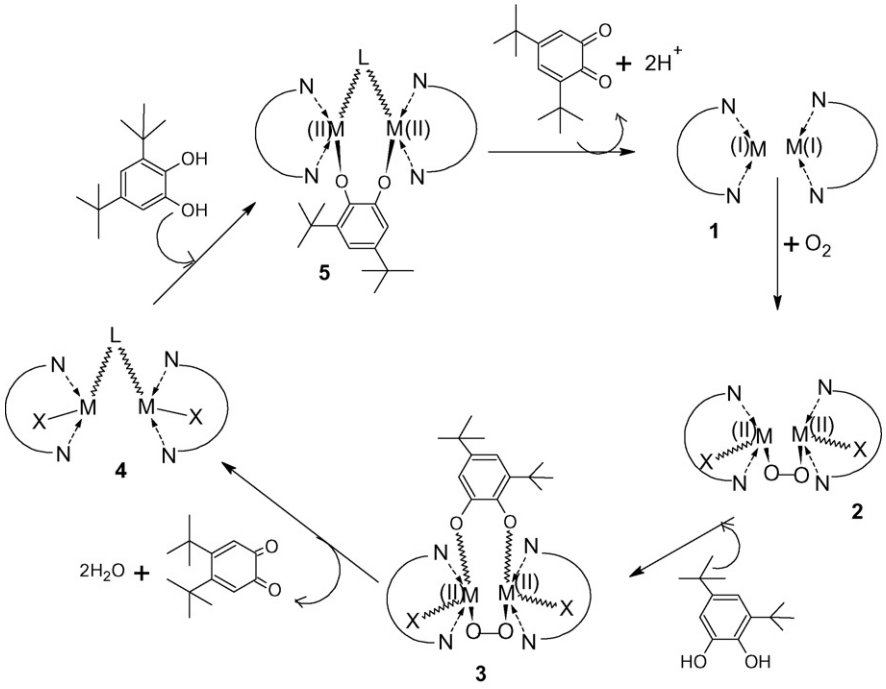

Scheme 1. L: The oxygen atom of the di-formylphenol fragment, X: the oxygen atom of the salicylidene moiety, M: Co(II). Suggested catalytic cycle for 3,5-DTBC.

Reaction of the ascorbic acid with the mono- and binuclear Co(II) and the $[Cu(H_2L)]Cl_2$ complexes were examined under nitrogen. The reduction process was monitored by measuring the changes in absorbance of the d–d bands of the complexes. The d–d bands of the complexes $[Co_2(L^1)]Cl$, $[Co_2(L^2)]Cl$ and $[Co(H_2L)]Cl_2$ in the range 655–643 and 613 nm for $[Cu(H_2L)]Cl_2$ disappear on addition of ascorbic acid under nitrogen, reappearing when the solution is exposed to air. It has been shown that only Cu^{II} complex with the tetrahedral structure are reduced to Cu^{I} by ascorbic acid. Planar Cu^{II} complexes are not reduced by these two-electron donors. Reduction of the Co(II) and Cu(II) complexes by ascorbic acid are therefore indirect evidence for the tetrahedral structure of the complexes. This has been inferred from spectral data. Moreover, the reduction process with ascorbic acid depend on the structure of the complexes. Binuclear and mononuclear Co(II) complexes are more active than the $[Cu(H_2L)]Cl_2$ complex. Also, the ligand H_3L^2 has more wide chelate ring ($n=3$) than the other ligands ($n=2$). Therefore, the complex $[Co_2(L^2)]Cl$ has highest activity against to the ascorbic acid. For the complexes, the activity order is:

$$[Co_2(L^2)]Cl > [Co_2(L^1)]Cl > [Co(H_2L)]Cl_2 > [Cu(H_2L)]Cl_2.$$

3.2. Kinetics of 3,5-di-tert-butylcatechol oxidation

The kinetics of the oxidation of 3,5-DTBC were determined by the method of initial rates by monitoring the growth of the 400 nm band of the product 3,5-DTBQ. To determine the dependence of the rates on the substrate concentration, solutions of the complexes $[Cu(H_2L)]Cl_2$, $[Co(H_2L)]Cl_2$, $[Co_2(L^1)]Cl$ and $[Co_2(L^2)]Cl$ were treated with increasing amounts of 3,5-DTBC. A first order dependence was observed at low concentrations of the substrate, whereas a saturation kinetic was found for all three compounds $[Co(H_2L)]Cl_2$, $[Co_2(L^1)]Cl$ and $[Co_2(L^2)]Cl$ at higher concentrations. A treatment on the basis of the Michaelis–Menten model, originally developed for enzyme kinetics, was applied. In our study, we can also propose a pre-equilibrium of free complex and substrate on the one hand, and a complex–substrate adduct on the other hand. The irreversible conversion into complex and quinone can be imagined as the rate-determining step. Although a much more complicated mechanism may be involved, the results show this simple model to be sufficient for a kinetic description. For the determination of the kinetic parameters for the three compounds studied the substrate rate was varied in the range from 1×10^{-3} to 1×10^{-4} mol dm^{-3} at a complex concentration of 1×10^{-4} mol dm^{-3}.

The observed kinetic behavior is consistent with the reaction mechanism (1)–(9).

$$Co^{II} + O_2 \rightarrow Co^{III}O_2 \quad (1)$$

$$Co^{III}O_2 + DBCatH_2 \rightarrow X \quad (2)$$

$$X \rightarrow Co^{III}O_2H + DBSQ^{\bullet -} + H^+ \quad (3)$$

$$Co^{II} + DBSQ^{\bullet -} \rightarrow Co^{III}(DBCatH) \quad (4)$$

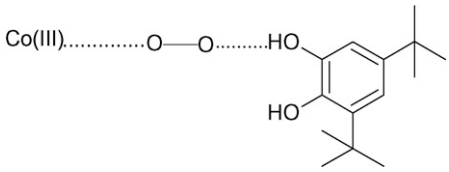

Fig. 3. Proposed structure of the intermediate X.

$$2Co^{II} + O_2 + DBCatH_2 \rightarrow Co^{III}(DBCatH) + Co^{III}O_2H \quad (5)$$

$$2Co^{III}O_2H \rightarrow 2Co^{III}OH + O_2 \quad (6)$$

$$Co^{III}OH + DBSQ^{\bullet -} + H^+ \rightarrow Co^{II} + DTBQ + H_2O \quad (7)$$

$$Co^{III}OH + Co^{III}(3,5\text{-}DBCatH) \rightarrow Co^{II} + Co^{III}(DBSQ^{\bullet -}) + H_2O \quad (8)$$

$$Co^{III}(DBSQ^{\bullet -}) \rightarrow Co^{II} + DTBQ \quad (9)$$

The kinetic behavior requires the formation of intermediate X (Fig. 3), which decomposes in the rate-determining H-atom abstraction step.

In the steady state following the fast initial phase, the overall stoichiometry requires that O_2 reduced to H_2O, rather than H_2O_2, therefore, the hydroperoxo Cosalen ($Co^{III}O_2H$) formed in step (3) should undergo disproportionation, regenerating one-half of the O_2 absorbed and producing the hydroxoCosalen ($Co^{III}OH$) (step (6)).

The hydrogen peroxide formation during the catalytic reaction was determined by iodometric titration [29]. Also, for a sustained catalytic cycle to occur in the steady state, a route to the product DTBQ and a path regenerating the Co(II) catalyst are necessary. These requirements of a catalytic cycle are fulfilled by addition of electron transfer steps (7) and (8) to the mechanism. The kinetics and mechanisms of the oxidations catalyzed by the Co(II) complexes are very similar. The kinetic results obtained for the systems studied are collected in Table 3. The plot of $\log(A_\infty/A_\infty - A_t)$ versus time for the catecholase activity of the complexes are shown in Fig. 4. The reactivity order (relative rate) for the Co(II) complexes is:

$$[Co_2(L^2)]Cl\,(32.74) > [Co_2(L^1)]Cl\,(30.58) > [Co(H_2L)]Cl_2\,(3.72).$$

We have also examined the catalytic activity of the mono- and binuclear complexes $[Co(H_2L)]Cl_2$, $[Co(H_2L)]Cl_2$,

Table 3
Kinetic properties of the mono- and binuclear complexes of the ligands H_2L, H_3L^1 and H_3L^2

Complex	Turnover-number (h^{-1})[a]
$[Cu(H_2L)]Cl_2$	No activity
$[Co(H_2L)]Cl_2$	3.72
$[Co_2(L^1)]Cl$	30.58
$[Co_2(L^2)]Cl$	32.74

[a] Turnover number is given as the number of moles converted or produced per unit weight and unit time.

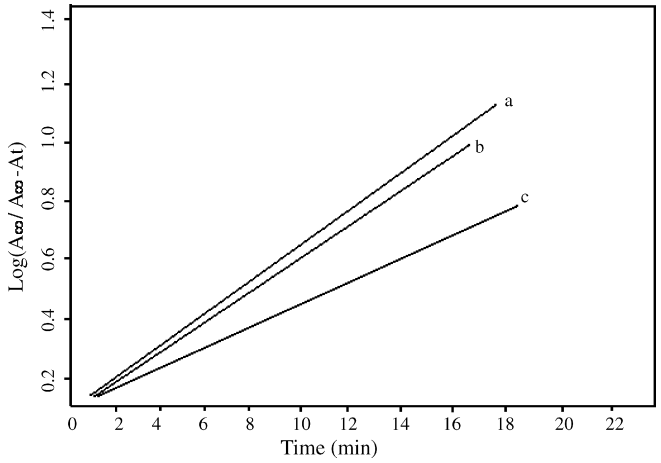

Fig. 4. Oxidation of catechol by the mono- and binuclear Co(II) complexes: (a) $[Co_2(L^1)]Cl$, (b) $[Co_2(L^2)]Cl$ and (c) $[Co(L)]_2Cl$.

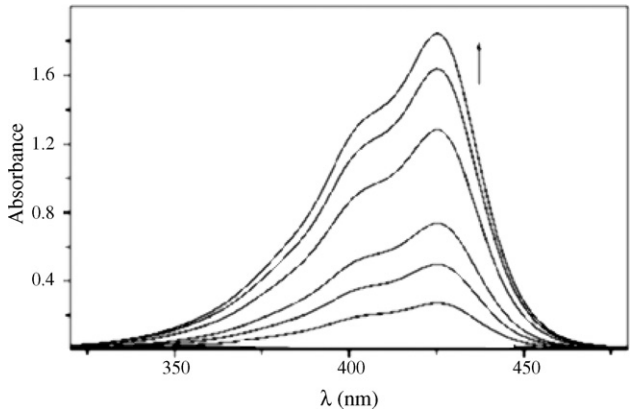

Fig. 6. Electronic spectra of the eluted solutions at different time intervals for the aerial oxidation of dtbp to TTBD by using complex $[Cu_2(L^2)]Cl$ as catalyst.

$[Co_2(L^1)]Cl$, $[Co_2(L^2)]Cl$, $[Cu_2(L^1)]Cl$ and $[Cu_2(L^2)]Cl$ for oxidation of 2,6-di-*tert*-butylphenol by air O_2 to 3,3′-5,5′-tetra-*tert*-butyl-4,4′-diphenolquinone (TTBD) in air saturated DCM according to the reaction in Fig. 5. All complexes in the catalysis reaction are soluble in the DCM-methanol solvent mixture. If they are not also soluble in this mixture, there is not any problem. Because, this type of reactions can occur at the heterogen or homogen phase in the similar way. As the oxidative carbon–carbon coupling of the sterically hindered phenol 2,6-di-*tert*-butylphenol leading to diphenoquinones is radical mediated reactions, we have studied the mono- and binuclear Co(II) and Cu(II) complexes for oxidative studies with 2,6-di-*tert*-butylphenol. When the phenol (2 mmol) is added to the complexes (0.01 mmol) in DCM–methanol (1:1) solvent mixture (50 mL), the dark brown or black colors of the solution turn to red or light red in presence of air. It was found that after 48 h, the phenol was converted to the 3,3′-5,5′-tetra-*tert*-butyl-4,4′-diphenolquinone.

The binuclear complexes are better oxidant than the mononuclear complexes. In addition, interestingly, the corresponding dicopper(II) complexes containing four radicals exhibit much less catechol oxidase activity than that of the corresponding dicobalt(II) complexes. For the compound 2,6-di-*tert*-butylphenol, the best oxidant is the complex of the ligand H_3L^2. Moreover, the complex of the ligand H_2L is the worst oxidant for the sterically hindered phenol. This different situation can be explained by the properties of the ligands and complexes. The Cu(II) complex of the ligand H_2L is mononuclear and has not any activity against the phenol. The reactivity order (relative rate) for the Co(II) and Cu(II) complexes is:

$$[Co_2(L^2)]Cl > [Co_2(L^1)]Cl > [Cu_2(L^2)]Cl > [Cu_2(L^1)]Cl > [Co(H_2L)]Cl_2.$$

The spectral properties of the complexes are shown in Fig. 5. The course of the reaction was followed by optical spectroscopy, as TTBD shows a characteristic peak in the electronic spectrum at 425 nm, as seen also from Fig. 6. Such changes in the electronic spectra of the complexes at different time intervals were monitored by removing the catalyst from the reaction solution. At the end of the oxidative coupling reaction, the properties of the complexes changed.

3.3. Electrochemical studies

A typical cyclic voltammograms of the complexes $[Ni_2(L^1)]Cl$, $[Ni_2(L^2)]Cl$ and $[Cu_2(L^1)]Cl$ are shown in Figs. 7–9 in MeCN containing 0.1 M $TBAClO_4$. For all the cyclic voltammograms at 100 mV s^{-1} scan rate, reduction at negative potential is the usual trend observed for phenoxo copper and nickel complexes because of the electronegativity and hard nature of the phenoxide atoms in the ligand. The initial

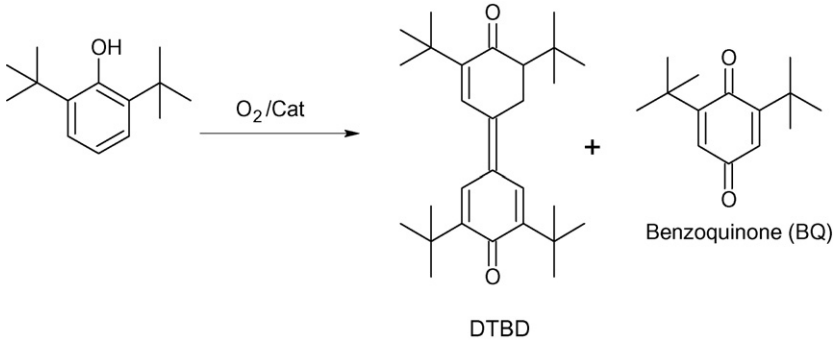

Fig. 5. Oxidative carbon–carbon coupling of the sterically hindered phenol 2,6-di-*tert*-butylphenol.

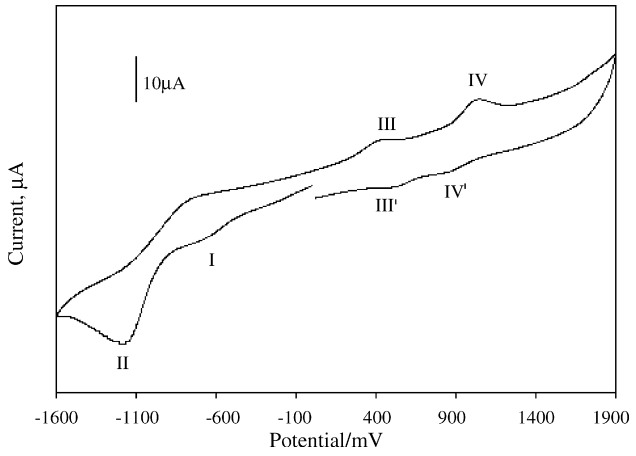

Fig. 7. Cyclic voltammogram for the reduction of the complex $[Cu_2(L^2)]Cl$ in MeCN containing 0.1 M $TBAClO_4$ at Pt disk electrode, scan rate 100 mV s^{-1}.

cathodic scan of the complex $[Cu_2(L^2)]Cl$ (Fig. 7) shows two reduction peaks, I (−680 mV) and II (−1200 mV). No oxidation peak corresponding to these waves were observed at this scan rate. This complex undergoes stepwise reductions at different potentials. This is similar to the behavior observed for related complexes [30]. In subsequent positive scans, two new redox couples were observed at the potentials 420 and 1020 mV (III and IV).

Coulometric experiments conducted at a potential −1150 mV than the second reduction wave indicate the consumption of two electrons per molecule. This indicates that the electron transfer may occur as follows:

$$\text{Cu(II)–Cu(II)} \xrightarrow{+e^-} \text{Cu(II)–Cu(I)} \xrightarrow{+e^-} \text{Cu(I)–Cu(I)}$$

These new peaks may be due to a chemical change occurring with the electron transfer. It depends on the structural reorganization in coordination sphere. The reduction potentials of the metal centers are influenced by the chelate ring size.

The electrochemical studies of similar types of complexes with hexa- and heptadentate coordination sites reported in the literature [31], suggest that the formal reduction potentials of

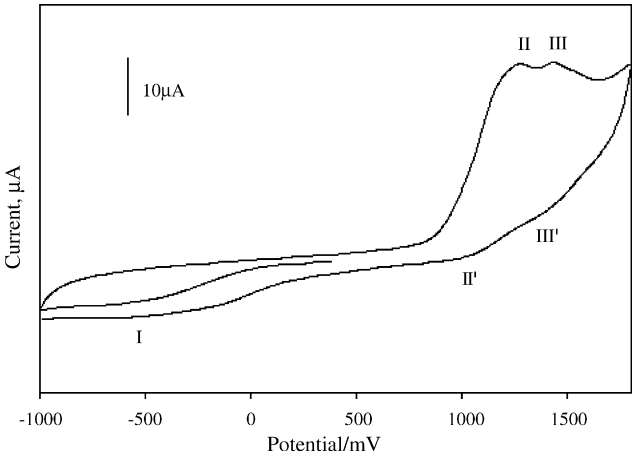

Fig. 8. Cyclic voltammogram of the complex $[Ni_2(L^1)]Cl$ in MeCN containing 0.1 M $TBAClO_4$ at Pt disk electrode, scan rate 100 mV s^{-1}.

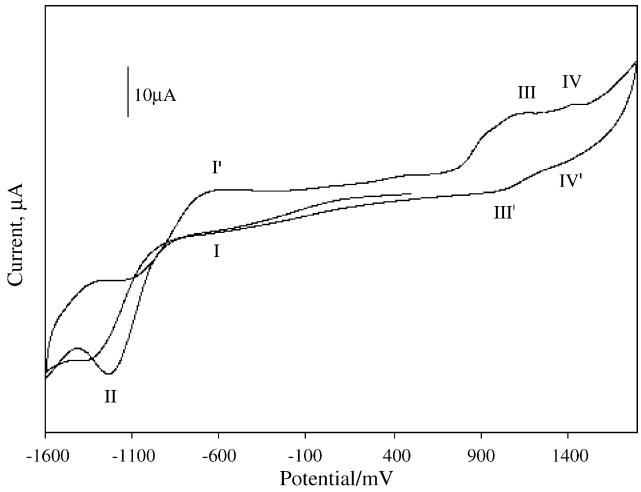

Fig. 9. Cyclic voltammogram of the complex $[Ni_2(L^2)]Cl$ in MeCN containing 0.1 M $TBAClO_4$ at Pt disk electrode, scan rate 100 mV s^{-1}.

the binuclear complexes may be assigned to the metal ion in the first binding site, that is the ethylene compartment. The second reduction potentials are comparable to that of the metal in the 6-coordination (N_4O_2) site.

For the binuclear complexes $[Ni_2(L^1)]Cl$ and $[Ni_2(L^2)]Cl$, similar voltammograms have been obtained in anhydrous acetonitrile solution containing 0.1 M $TBAClO_4$ at a platinum disc electrode. In the complex $[Ni_2(L^1)]Cl$ (Fig. 8), one irreversible reduction peak (I) at −480 mV versus Ag/AgCl could be seen. In the positive sweep, two quasireversible oxidation peaks appear at 1275(II) and 1433(III) mV. Fig. 9 shows the cyclic voltammogram of complex $[Ni_2(L^2)]Cl$. This cyclic voltammogram has a similar voltammetric behavior as the $[Ni_2(L^1)]Cl$ complex. However, a new irreversible wave at −1235 mV is appeared. In both cases, the complexes exhibit cathodic reduction peaks in the range of 450–480 mV versus Ag/AgCl, probably corresponding to a process involving Ni^0 at the electrode surface. These reduction potentials, however, do differ the reported value of +360 mV versus SCE for the enzyme tyrosinase isolated from mushrooms.

The cyclic voltammogram of the complex $[Cu(H_2L)]Cl_2$ shows a irreversible reduction at $E_{pc} = -0.700$ and −0.842 V versus Ag/AgCl, which can be ascribed to the $Cu^{2+} \rightarrow Cu^+$ process. The reduction process is irreversible for the Cu(II) complex, and leads to a deposit of copper(0) on the electrode surface, as judged by the observation of a sharp oxidation peak during the reverse scan.

3.4. Antimicrobial studies

The biological activity of the three Schiff base ligands (H_2L, H_3L^1 and H_3L^2) and their complexes were tested against the bacteria and yeast because bacteria can achieve resistance to antibiotics through biochemical and morphological modifications [30]. The organisms used in the present investigations included *C. xerosis*, *B. brevis*, *B. megaterium*, *B. cereus*, *M. smegmatis*, *S. aureus*, *M. luteus* and *E. faecalis* (as Gram-positive bacteria) and *P. aeruginosa*, *K. pneumoniae*, *E. coli*, *Y. enterocolitica*, *Kluyveromyces fragilis*, *S. cerevisiae*, *C. albicans* (as

Table 4
Antimicrobial activity data for the selected some Schiff base complexes

Microorganisms	CFU[a]/mL inoculum	Inhibition zone (mm)										
		1	2	3	4	5	6	7	8	A10[b]	S10[c]	N100[d]
Gram-positive bacteria												
Corynebacterium xerosis	6.9×10^8	24[e]	7	30	20	10	[f]	24	12	12	10	NT
Bacillus brevis	7.6×10^8	20	20	27	25	27	17	23	10	14	16	NT
Bacillus megaterium	8.3×10^7	35	18	28	28	17	15	29	17	11	17	NT
Bacillus cereus	5.8×10^8	34	18	30	30	30	20	24	7	15	18	NT
Mycobacterium smegmatis	6.9×10^8	27	20	24	29	28	24	30	22	19	15	NT
Staphylococcus aureus	9.7×10^7	33	18	27	30	20	20	24	22	25	22	NT
Micrococcus luteus	5.5×10^8	30	17	30	27	28	22	30	11	33	–	NT
Enterococcus faecalis	6.6×10^8	25	23	27	29	26	16	28	23	16	17	NT
Gram-negative bacteria												
Pseudomonas aeruginosa	5.6×10^8	35	18	26	28	30	20	26	8	10	13	NT
Klebsiella pneumoniae	8.7×10^8	33	15	25	27	25	22	25	11	17	16	NT
Escherichia coli	9.6×10^7	24	18	30	24	26	21	28		13	17	NT
Yersiniaenterocolitica	6.4×10^8	30	12	26	23	–	14	25	18	13	17	NT
Kluyveromyces fragilis	7.6×10^8	28	13	30	15	31	16	16	14	NT	NT	15
Saccharomyces cerevisiae	5.0×10^8	30	16	30	28	28	20	30	15	NT	NT	14
Candida albicans	6.9×10^8	30	30	30	30	27	14	30	12	NT	NT	19

[a] Number of colony forming units.
[b] Ampicillin (10 μg/disc).
[c] Streptomycin (10 μg/disc).
[d] Nystatin 100 Units (10 μg/disc).
[e] Inhibition zone (mm).
[f] No inhibition zone is determined. Blanks mean not investigated. NT: not tested. 1: $[Cd_2(L^1)]Cl$, 2: $[Ni_2(L^1)]Cl$, 3: $[Co_2(L^1)]Cl$, 4: $[Cu_2(L^1)]Cl$, 5: $[Cu_2(L^2)]Cl$, 6: $[Ni_2(L^2)Cl]$, 7: $[Co_2(L^2)Cl]$, 8: $[Cd_2(L^2)]Cl$.

Gram-negative bacteria). The diffusion agar technique was used to evaluate the antibacterial activity of the synthesized complexes.

The results of the bactericidal screening of the synthesized compounds are recorded in Table 4. The Schiff base ligands H_2L, H_3L^1 and H_3L^2 have moderate activity in comparison with *Staphylococcus aureus*, *Escherichia coli* and less active in comparison with *P. aeruginosa*. The remarkable activity of the Schiff base ligands may be arise from the hydroxyl groups, which may play an important role in the antibacterial activity, as well as the presence of four imine groups which imports in elucidating the mechanism of transformation reaction in biological systems. The activity of the two Schiff base ligands and their complexes increases as the concentration increases because it is a well known fact that concentration plays a vital role in increasing the degree of inhibition. The results indicate that the complexes show more activity and the ligands do not have any activity against same microorganisms under identical experimental conditions. This would suggest that the chelation could facilitate the ability of a complex to cross a cell membrane and can be explained by Tweedy's chelation theory [32]. Chelation considerably reduces the polarity of the metal ion because of partial sharing of its positive charge with donor groups and possible electron delocalization over the whole chelate ring. Such a chelation could enhance the lipophilic character of the central metal atom, which subsequently favors its permeation through the lipid layer of the cell membrane. The variation in the effectiveness of different compounds against different organisms depends either on the impermeability of the cells of the microbes or on differences in ribosome of microbial cells. The activity of the Schiff base ligands and their metal complexes increases as the concentration increases because it is a well known fact that concentration plays a vital role in increasing the degree of inhibition. Almost all compounds (except the complexes $[Cu_2(L^2)]Cl$ and $[Ni_2(L^2)]Cl$ have not activity against the *Y. enterocolitica* and *C. xerosis*, respectively) have activity against the bacteria and yeasts. The complex $[Cd_2(L^1)]Cl$ has highest activity against the *B. megaterium* and *P. aeruginosa* (bacteria) and *S. cerevisiae* and *C. albicans* (yeast). In other words, the antibiotic nystatin is the standard antifungal. Therefore, it did not test against the all bacteria. The nystatin was only tested for the three yeasts and obtained results are low. In like manner, the ampicillin and streptomycin are antibacterial drugs and have been only tested against the bacteria. The streptomycin does not show any activity against the *M. luteus*.

3.5. Thermogravimetric studies

In order to give more insight into the structure of the complexes, the thermal studies of the complexes have been carried out using thermogravimetry (DTA-TG) techniques. The thermogravimetric studies have been made in the temperature range 20–850 °C. All complexes have a similar decomposition process. Thermal decomposition takes places in two steps. In the first step, the thermogravimetric analysis (TGA) indicates loss of one chloride ion in the range of 180–220 °C for the complexes (in the binuclear complexes 1 mol chloride ion and in the mononuclear complexes 2 mol of chloride ion). Loss of chloride ion as HCl at the low temperatures indicates that the chloride ions are not coordinated to the metal ions. This is in

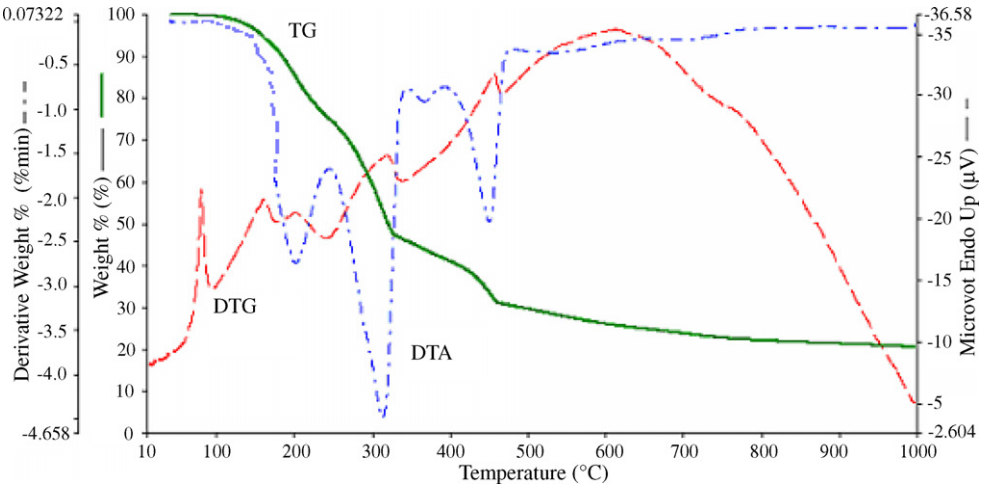

Fig. 10. Thermal analyses curves of the binuclear complex $[Cu_2(L^1)]Cl$.

agreement with C, H, N analysis presented in Table 1. The thermogravimetric analysis revealed that the complex loses mass between 180 and 220 °C, corresponding to 13.64% of the total mass. In the second step, the remaining metal complexes by loss of the outside chloride ion(s) decompose to the metal oxide $[(M_xO_y)$ (x: 3, y: 4 for Co(II) and Ni(II); x: 1, y: 1 for Cu(II)] at the higher temperatures up to 850 °C. The percentage ratio of the metal oxides fits well with the proposed formula.

Differential thermal analyses of the complexes have similar properties. In all complexes, the loss of the chloride ion as HCl is endothermic process and metal oxide formation process is exothermic. In Fig. 10, the thermal decomposition steps of the binuclear complex $[Cu_2(L^1)]Cl$ is shown. As seen from Fig. 10, the complex does not contain any hydrated or adsorbed water molecules. Decomposition process starts approximately at the ~180 °C temperature and continues to the higher temperatures. The final product of the decomposition process is the metal oxide.

Acknowledgements

This work was supported by K. Maras Sütçü Imam University, Head of Research Unit (Project code: 2003/7-5). Thanks are also due to the referees for their valuable comments. We thank Dr. Metin Dığrak (K. Maraş Sütçü Imam University, Biology Department) for the antimicrobial activity tests. We also thank the Cukurova University for thermal analyses and the Atatürk University for NMR and electrochemical studies, respectively.

References

[1] (a) B.O. West, J. Chem. Soc. (1952) 3115;
(b) B.O. West, J. Chem. Soc. (1960) 4944;
(c) A. van den Bergen, K.S. Murray, M.J. O'Connor, B.O. West, Aust. J. Chem. 22 (1969) 39.
[2] S. Yamada, E. Ohno, K. Yamanouchi, Bull. Chem. Soc. Jpn. 41 (1968) 535.
[3] E.C. Niederhoffer, J.H. Timmons, A.E. Martell, Chem. Rev. 84 (1984) 137.
[4] (a) A. Bencini, A. Bianchi, C. Giorgi, P. Paoletti, B. Valtancoli, N. Ceccanti, R. Pardini, Polyhedron 19 (2000) 2441;
(b) N. Ceccanti, R. Pardini, F. Secco, M.R. Tine, M. Venturini, A. Bianchi, P. Paoletti, Polyhedron 19 (2000) 2447.
[5] W. Kaim, J. Rall, Angew. Chem. 35 (1996) 43.
[6] (a) K.A. Magnus, H. Ton-That, J.E. Carpenter, Chem. Rev. 94 (1994) 727;
(b) R.S. Himmelwright, N.C. Eickman, C.D. Lubien, E.I. Solomon, J. Am. Chem. Soc. 102 (1980) 5378.
[7] (a) T.B. Freedman, J.S. Loehr, T.M. Loehr, J. Am. Chem. Soc. 98 (1976) 2809;
(b) T.J. Thamann, J.S. Loehr, T.M. Loehr, J. Am. Chem. Soc. 99 (1977) 4187;
(c) J.A. Larrabee, T.G. Spiro, N.S. Ferris, W.H. Woodruff, W.A. Maltese, M.S. Kerr, J. Am. Chem. Soc. 99 (1977) 1979;
(d) J.A. Larrabee, T.G. Spiro, J. Am. Chem. Soc. 102 (1980) 4217.
[8] H.S. Mason, W.L. Fowlks, E. Peterson, J. Am. Chem. Soc. 77 (1955) 2914.
[9] M. Tremolieres, J.B. Bieth, Phytochemistry 23 (1984) 501.
[10] G.S. Patterson, R.H. Holm, Bioinorg. Chem. 4 (1975) 257.
[11] D.B. Rorabacher, M.J. Martin, M.J. Koenigbauer, M. Malik, P.R. Schroeder, J.F. Eudicott, L.A. Ochrymowyez, in: K.D. Karlin, J. Zubieta (Eds.), Copper Coordination Chemistry: Biochemical and Inorganic Perspectives, Academic Press, New York, 1983.
[12] R.S. Drago, M.J. Desmond, B.B. Corden, K.A. Miller, J. Am. Chem. Soc. 105 (1983) 2287.
[13] G.H. Jeffrey, J. Basset, J. Mendham, R.J. Denny, Vogel's Quantitative Chemical Analysis, fifth ed., Longmand Science and Tech, Sussex, UK, 1989, p. 447.
[14] D.M. Boghaei, M. Lashanizadegan, Synth. React. Inorg. Met. Org. Chem. 30 (2000) 1393.
[15] D.M. Boghaei, S.J.S. Sabounchei, S. Rayati, Synth. React. Inorg. Met. Org. Chem. 30 (2000) 1535.
[16] C.H. Collins, P.M. Lyne, J.M. Grange, Microbiological Methods, Butterworths & Co. Ltd., London, UK, 1989.
[17] L.J. Bradshaw, Laboratory Microbiology, fourth ed., Saunders College Publishing, USA, 1992.
[18] M. Tümer, C. Çelik, H. Köksal, S. Serin, Trans. Met. Chem. 24 (5) (1999) 525.
[19] M. Tümer, H. Köksal, S. Serin, M. Dığrak, Trans. Met. Chem. 24 (1) (1999) 13.
[20] H. Köksal, M. Dolaz, M. Tümer, S. Serin, Synth. React. Inorg. Met. Org. Chem. 31 (2001) 1141.
[21] R. Atkins, G. Brewer, E. Kokot, G.M. Mockler, E.J. Sinn, J. Inorg. Chem. 24 (1985) 127.
[22] A.L. Nivorozhkin, H. Toflund, P.L. Jorgensen, L.E. Nivorozhkin, J. Chem. Soc. Dalton Trans. (1996) 1215.
[23] W.J. Geary, Coord. Chem. Rev. 7 (1971) 81.

[24] M. Tümer, H. Köksal, S. Serin, Synth. React. Inorg. Met. Org. Chem. 27 (1997) 775.
[25] (a) M. Dolaz, M. Tümer, Trans. Met. Chem. 29 (2004) 516;
(b) M. Dolaz, M. Tümer, M. Dığrak, Trans. Met. Chem. 29 (2004) 528.
[26] A.M. Mayer, Phytochemistry 1 (1962) 23.
[27] G. Lanzarini, P.G. Pifferi, A. Zamorani, Phytochemistry 11 (1972) 89.
[28] (a) P. Baruah, T. Swain, J. Sci. Food Agric. 10 (1959) 125;
(b) J.R.L. WaJker, Enyme Technol. Dig. 4 (1975) 89.
[29] M.G. Karmarkar, C.S. Pandav, K.A.V.R. Krishnamachari, Principle and Procedure for Iodine Estimation: A Laboratory Manual, Indian Council of Medical Research, New Delhi, 1986.
[30] S. Mandal, K. Nag, J. Chem. Soc. Dalton Trans. (1983) 2429.
[31] (a) C. Fraser, B. Bosnich, Inorg. Chem. 41 (2002) 1788;
(b) E. Chartone-Souza, T.L. Loyola, M.B. Rodriguez, M.-A. de B.C. Menezes, N.A. Rey, E.C. Pereira-Maia, J. Inorg. Biochem. 99 (2005) 1001.
[32] B.G. Tweedy, Phytopathalogy 55 (1964) 910.